

The identification of post-starburst galaxies at $z \sim 1$ using multiwavelength photometry: a spectroscopic verification

David T. Maltby^{1*}, Omar Almaini¹, Vivienne Wild^{2,3}, Nina A. Hatch¹,
William G. Hartley⁴, Chris Simpson, Ross J. McLure³, James Dunlop³,
Kate Rowlands² and Michele Cirasuolo⁵

¹*School of Physics and Astronomy, University of Nottingham, University Park, Nottingham, NG7 2RD, UK*

²*School of Physics and Astronomy, University of St Andrews, North Haugh, St Andrews, KY16 9SS, UK (SUPA)*

³*Institute for Astronomy, University of Edinburgh, Royal Observatory, Blackford Hill, Edinburgh, EH9 3HJ, UK (SUPA)*

⁴*ETH Zürich, Institut für Astronomie, Wolfgang-Pauli-Str. 27, CH-8093 Zürich, Switzerland*

⁵*UK Astronomy Technology Ctr., Royal Observatory, Blackford Hill, Edinburgh, EH9 3HJ, UK*

Accepted yyyy mm dd. Received yyyy mm dd; in original form yyyy mm dd

ABSTRACT

Despite decades of study, we still do not fully understand why some massive galaxies abruptly switch off their star formation in the early Universe, and what causes their rapid transition to the red sequence. Post-starburst galaxies provide a rare opportunity to study this transition phase, but few have currently been spectroscopically identified at high redshift ($z > 1$). In this paper we present the spectroscopic verification of a new photometric technique to identify post-starbursts in high-redshift surveys. The method classifies the broad-band optical–near-infrared spectral energy distributions (SEDs) of galaxies using three spectral shape parameters (super-colours), derived from a principal component analysis of model SEDs. When applied to the multiwavelength photometric data in the UKIDSS Ultra Deep Survey (UDS), this technique identified over 900 candidate post-starbursts at redshifts $0.5 < z < 2.0$. In this study we present deep optical spectroscopy for a subset of these galaxies, in order to confirm their post-starburst nature. Where a spectroscopic assessment was possible, we find the majority (19/24 galaxies; ~ 80 per cent) exhibit the strong Balmer absorption ($H\delta$ equivalent width $W_\lambda > 5 \text{ \AA}$) and Balmer break, characteristic of post-starburst galaxies. We conclude that photometric methods can be used to select large samples of recently-quenched galaxies in the distant Universe.

Key words: methods: statistical — galaxies: fundamental parameters — galaxies: high-redshift — galaxies: photometry — galaxies: statistics — galaxies: stellar content.

1 INTRODUCTION

Deep surveys have transformed our view of the distant Universe, allowing us to observe the process of galaxy assembly over the last 13 billion years of cosmic history. However, despite much progress, many crucial aspects of galaxy formation and evolution remain poorly understood. In particular, we still do not understand the mechanisms responsible for quenching star formation in massive galaxies, as required to produce both the ‘red nuggets’ observed at high redshift (e.g. Trujillo et al. 2006) and the quiescent galaxies we observe today (e.g. Baldry et al. 2004).

To terminate star formation in galaxies, several mechanisms have been proposed. These include, gas stripping (e.g. Gunn & Gott 1972), morphological quenching (Martig et al. 2009), AGN or starburst-driven superwinds (Hopkins et al. 2005; Diamond-Stanic et al. 2012), shock heating of infalling cold gas by

the hot halo (Dekel & Birnboim 2006), and an exhaustion of the gas supply (e.g. Larson et al. 1980). Furthermore, to keep star formation suppressed, radio-mode AGN feedback may also be required (Best et al. 2005).

To disentangle the relative roles of these processes at high redshift, we require a large sample of galaxies that are caught in the act of transformation. The rare class of ‘post-starburst’ galaxies is potentially ideal for such studies. Otherwise known as ‘E+A’ or ‘k+a’ galaxies, post-starbursts represent transition systems in which a major burst of star formation was quenched within the last few hundred Myr, leaving a characteristic A-star imprint of strong Balmer lines on an otherwise passive-looking galaxy spectrum (Dressler & Gunn 1983; Wild et al. 2009). However, due to their very red spectral energy distributions (SEDs) and intrinsic short-lived nature, only a handful have been spectroscopically identified at $z > 1$; e.g. 3 galaxies in zCOSMOS (Vergani et al. 2010) and 5 galaxies in the spectroscopic component of the Ultra Deep Survey (UDSz; Wild et al. 2014).

* E-mail: dtmaltby@gmail.com

In order to increase the number of post-starburst (PSB) galaxies identified at high redshift, two photometric methods have recently been developed. [Whitaker et al. \(2012\)](#) use medium-band infrared imaging to identify ‘young red-sequence’ galaxies via rest-frame *UVJ* colour-colour diagrams. [Wild et al. \(2014\)](#), however, use an alternative approach and classify galaxies based on a principal component analysis (PCA) of their SEDs. When this latter method is applied to the multiwavelength photometry of the Ultra Deep Survey (UDS; [Almaini et al., in preparation](#)), it transpires that just three shape parameters (i.e. eigenspectra) provide a compact representation of a wide variety of SED shapes. This enables the identification of several galaxy populations, including PSBs which have formed > 10 per cent of their mass in a recently-quenched starburst event.

Using photometry for over 130000 *K*-band selected UDS galaxies, this PCA method has identified over 900 candidate PSBs at $0.5 < z < 2.0$ ([Wild et al., in preparation](#)). Such a large sample of high-redshift post-starbursts will enable a wide range of scientific studies and provide crucial insight into the quenching of star formation in galaxies at high redshift. At present, however, the spectroscopic confirmation rests on a limited number of low-resolution spectra from UDSz (5 PSBs; [Wild et al. 2014](#)). In this study, we provide a more robust assessment using medium-resolution deep-optical spectroscopy for a much larger sample of PSB candidates. This provides the crucial validation required to unlock a wealth of science on high-redshift post-starbursts selected from the UDS and other photometric surveys.

The structure of this paper is as follows. In Section 2, we give a brief description of the UDS data and VIMOS spectroscopy upon which this work is based, outlining the photometric identification of PSB candidates and our selection of spectroscopic targets in Section 2.2. In Section 3, we present the reduced VIMOS spectra for PSB candidates and classify the galaxies using standard spectroscopic criteria. Finally, we draw our conclusions in Section 4.

2 DESCRIPTION OF THE DATA

2.1 The Ultra Deep Survey (UDS)

The UDS is the deepest component of the UKIRT (United Kingdom Infra-Red Telescope) Infrared Deep Sky Survey (UKIDSS; [Lawrence et al. 2007](#)) and the deepest degree-scale near-infrared survey to date¹. The survey comprises extremely deep UKIRT *JHK* photometry, covering an area of 0.77 deg^2 . The work presented here is based on the eighth UDS data release (DR8) where the limiting depths are $J = 24.9$; $H = 24.4$ and $K = 24.6$ (AB; 5σ in 2 arcsec apertures). In addition, the UDS is complemented by extensive multiwavelength observations including deep-optical *BVRi'z'* photometry from the Subaru-*XMM-Newton* Deep Survey (SXDS; [Furusawa et al. 2008](#)) and mid-infrared coverage (3.6 and $4.5 \mu\text{m}$) from the *Spitzer* UDS Legacy Program (SpUDS; PI: Dunlop). Furthermore, deep *u'*-band photometry is also available from the Canada-France-Hawaii Telescope (CFHT) Megacam. The complete extent of the UDS field with full multiwavelength coverage (optical-mid-infrared) is $\sim 0.62 \text{ deg}^2$. For a complete description of these data, including a description of the catalogue construction, see [Hartley et al. \(2013\)](#) and [Simpson et al. \(2012\)](#). In this work, where appropriate, we use the photometric redshifts described in [Simpson et al. \(2013\)](#).

¹ <http://www.nottingham.ac.uk/astronomy/UDS/>

2.2 The super-colour method and target selection

To identify high-redshift PSB candidates in the UDS, we use the PCA technique of [Wild et al. \(2014\)](#). We provide a brief description of the method below.

[Wild et al. \(2014\)](#) begin by building a large library of ~ 44000 ‘stochastic burst’ model SEDs, generated from [Bruzual & Charlot \(2003\)](#) stellar population synthesis models with stochastic star-formation histories. These model SEDs are convolved with the photometric filter set of the UDS and progressively shifted to cover the redshift range of interest (e.g. $0.5 < z < 2.0$). A PCA analysis is then applied to all model SEDs in order to establish a mean SED (m_λ) and a series of p eigenvectors (eigenspectra; $e_{i\lambda}$) from which any normalised SED (f_λ/n) can be approximately reconstructed:

$$\frac{f_\lambda}{n} = m_\lambda + \sum_{i=1}^p a_i e_{i\lambda}. \quad (1)$$

The principal component amplitudes (a_i), indicate the ‘amount’ of each eigenspectrum contained within a galaxy’s SED and can be used to uniquely define its shape. Referred to as *super-colours* (SCs), these amplitudes combine data from multiple filters using an optimally defined weighting scheme (the eigenspectra) and allow for all key information available from multiwavelength photometry to be retained. In fact, it transpires that only the first three SCs ($a_1 = \text{SC1}$; $a_2 = \text{SC2}$; $a_3 = \text{SC3}$) are required in order to provide a compact representation of a wide variety of SED shapes, accounting for > 99.9 per cent of the variance in the models of [Wild et al. \(2014\)](#). For these SCs, several useful correlations exist with the star-formation histories of the model SEDs. For example, SC1 correlates with both mean stellar age and dust content; SC2 and SC3 correlate with metallicity; and SC2 correlates with the fraction of stellar mass formed in bursts in the last Gyr. These key correlations enable the separation of a tight red-sequence from star-forming galaxies and also help identify three unusual populations: very dusty star-forming galaxies, metal poor quiescent dwarf galaxies, and PSBs that have formed > 10 per cent of their mass in a recently-quenched starburst (see [Wild et al. 2014](#)).

For real galaxies, a PCA analysis is used to project their SEDs into SC space, with a comparison to the SCs of the model SEDs used in order to determine their probable nature (e.g. red-sequence, star-forming, PSB). The benefit of this approach is that no model SED or *K*-correction is assumed in determining the SCs of the actual galaxies themselves. In the UDS, this PCA analysis was performed using 8 UDS filters (*VRi'z'JHK*, $3.6 \mu\text{m}$), and on all galaxies with $K_{\text{AB}} < 24$ and $0.5 < z < 2.0$ (48713 galaxies; [Wild et al., in preparation](#)). From this analysis, a parent sample of 4249 red-sequence galaxies, 39970 star-forming galaxies and 921 PSB candidates have been identified.

To verify the identification of PSB galaxies, we select spectroscopic targets from this parent sample covering a wide range in redshift and magnitude (see Fig. 1). Note, however, that selection was based on preliminary catalogues to a limit of $K_{\text{AB}} < 23$, and that targets were chosen with $i < 24.5$ to ensure adequate signal-to-noise (S/N) in the optical spectra. Red-sequence galaxies were also selected, with priority given to those near the SC classification boundary with post-starbursts, to allow for a robust calibration of the boundary’s position. A total of 88 targets were selected, including 37 PSB candidates and a comparison sample of 34 red-sequence galaxies. Spectra for an additional 11 star-forming, 2 dusty star-forming and 4 low-metallicity galaxies were also taken, but these are not considered in this paper.

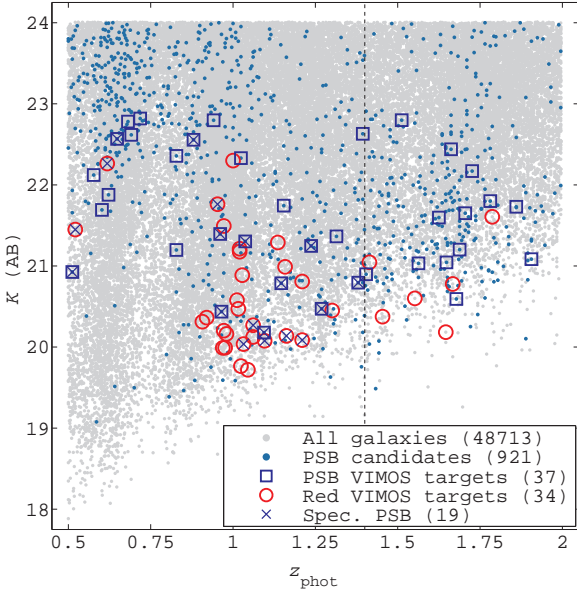


Figure 1. K -band magnitude versus photometric redshift for UDS galaxies ($0.5 < z < 2.0$; $K_{AB} < 24$), showing the super-colour selected post-starburst (PSB) candidates (blue points). Spectroscopic targets from our new medium-resolution spectroscopy (see Section 2.3) are shown: PSB candidates (blue squares) and red-sequence galaxies (red circles). Respective sample sizes are shown in the legend. Also indicated are the upper redshift limit for our spectroscopic PSB classification ($z = 1.4$; black dashed line) and the PSBs identified from the spectroscopy of these targets (blue crosses; see Section 3 and Table 1). Note that spectroscopic candidates were selected from an early version of the SC catalogue to $K_{AB} < 23$.

2.3 VIMOS spectroscopy and data reduction

Spectroscopic observations were taken with the VIMOS spectrograph at the European Southern Observatory’s Very Large Telescope (ESO programme 094.A-0410). Observations were performed in multi-object spectroscopy (MOS) mode. Spectroscopic data were taken with a single VIMOS mask and with total on-source exposures of ~ 4 h, which were divided over 7 observing blocks (OBs) and four nights (data taken in Nov/Dec 2014). Each individual OB had an exposure time of ~ 35 min (2088s) and was observed in a pattern of three 1.2 arcsec dithered exposures. All observations were performed in dark time, under clear conditions, with a seeing of < 1 arcsec and with an airmass < 1.2 . Standard calibration data were also taken as part of the observing programme; including detector biases, screen flat fields, arc-lamp exposures and spectro-photometric standards.

We use VIMOS with the medium-resolution grism (MR) and GG475 order sorting filter; a configuration that provides a wide wavelength coverage (4800–10000 Å) and a dispersion of $2.6 \text{ \AA pixel}^{-1}$. The field of view for VIMOS is separated into four quadrants, each of which is $7 \times 8 \text{ arcmin}^2$. For our MOS observations, we use slit masks with 20–25 slits per quadrant, yielding spectra for a total of 88 galaxies in the UDS field (see Section 2.2). The masks use slits of 1 arcsec width, resulting in a typical spectral resolution of $R = 580$.

Raw spectra were reduced using the VIMOS MOS pipeline (version 2.9.16) and within the ESO REFLEX environment (Freudling et al. 2013). Standard data reduction procedures were followed, leading to flux- and wavelength-calibrated spectra with a mean rms in the residuals of the wavelength calibration $< 0.7 \text{ \AA}$.

Finally, the 1-D spectra for each individual target from all 7 OBs were normalised and combined in a median stack.

From the reduced spectra, we determine spectroscopic redshifts z_{spec} using the EZ and SGNAPS packages (Garilli et al. 2010; Paoro & Franzetti 2012). With EZ, redshifts are determined using a cross-correlation of spectral templates. Here we use the default templates, but also include the additional templates of Bradshaw et al. (2013), constructed for UDSz. Optimal solutions were confirmed via spectral line identification in SGNAPS. Overall, the spectra had sufficient S/N to determine z_{spec} in ~ 70 per cent of cases.

3 RESULTS

To confirm the nature of our PSB candidates, we determine the presence of strong Balmer absorption lines (e.g. $H \delta \lambda 4102 \text{ \AA}$) combined with a strong Balmer break (Wild et al. 2009). An equivalent width in $H \delta > 5 \text{ \AA}$ is generally considered diagnostic of a PSB galaxy (although often combined with a lack of significant emission lines; e.g. Goto 2007). Equivalent width (W_λ) is defined as

$$W_\lambda = \int_{\lambda_1}^{\lambda_2} 1 - F(\lambda)/F_c(\lambda) d\lambda, \quad (2)$$

where $F(\lambda)$ is the spectral flux and $F_c(\lambda)$ is the continuum emission. We compute the rest-frame $H \delta$ equivalent width ($W_{H\delta}$) using a non-parametric approach based on that used by previous works (e.g. Goto et al. 2003). First, z_{spec} is used to transform the spectrum into the rest-frame. Then continuum emission is estimated across $H \delta$ using a linear interpolation between the continuum measured in narrow intervals on either side (4030–4082 and 4122–4170 Å). These intervals are chosen for their lack of significant absorption/emission lines and their continuum is modelled by a linear regression that includes both intervals, weighted by the inverse square error in the flux. A $3\text{-}\sigma$ rejection to deviant points above/below an initial continuum model is also used to minimise the effect of noise. Finally, $W_{H\delta}$ is determined using the ratio $F(\lambda)/F_c(\lambda)$ across an interval that encapsulates $H \delta$ ($\lambda_1 = 4082$ to $\lambda_2 = 4122 \text{ \AA}$).

In this study, the need to identify $H \delta$ ($\lambda 4102 \text{ \AA}$) restricts unambiguous PSB classification to $z < 1.4$, where $H \delta$ is within spectral reach of VIMOS. This is the case for 24/37 of our PSB candidates (see Fig. 1). In this regime, due to the faintness of our targets the S/N was only sufficient for a secure z_{spec} and $W_{H\delta}$ measurement in 15/24 of cases. For one of these cases, an anomaly in the continuum region made the measurement of $W_{H\delta}$ problematic, possibly due to a close/projected companion. This candidate is consequently removed from our sample. From the remaining ‘good’ candidates, we find that the majority (11/14; ~ 80 per cent) do exhibit the strong Balmer absorption ($W_{H\delta} > 5 \text{ \AA}$) and a Balmer break, characteristic of PSB galaxies. This result demonstrates the overall effectiveness of the Wild et al. (2014) PCA technique for selecting high-redshift post-starbursts at $z < 1.4$. For the three candidates that were not confirmed, all exhibit significant but weaker $H \delta$ absorption ($W_{H\delta} \sim 3 \text{ \AA}$). Details of our confirmed PSBs, including their diagnostic $W_{H\delta}$, are presented in Table 1.

We also determine $W_{H\delta}$ for our red-sequence targets. Of the cases where a measurement was possible (26/34 galaxies), we confirm that the majority (18/26; ~ 70 per cent) exhibit either very weak or insignificant $H \delta$ absorption ($W_{H\delta} < 5 \text{ \AA}$; see Fig. 2, for examples). For the remaining cases (8 galaxies; ~ 30 per cent), post-starburst signatures were actually observed ($W_{H\delta} > 5 \text{ \AA}$; see Table 1). Some overlap between the populations is not surprising, however, since photometric methods for identifying PSBs will be less sensitive to post-starburst signatures than using spectroscopy.

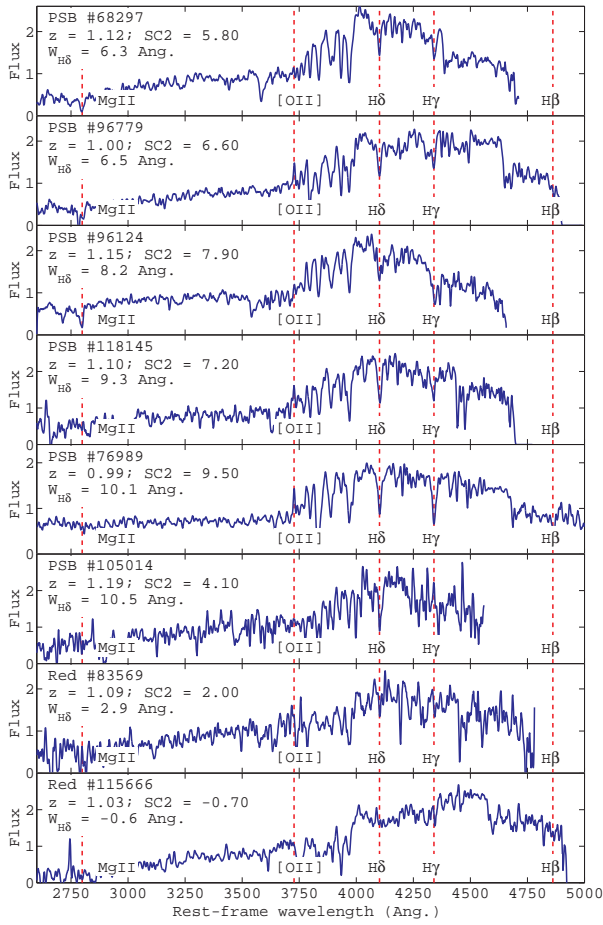


Figure 2. Example VIMOS spectra for post-starburst (PSB) and red-sequence galaxies in the UDS. The PSBs all exhibit the strong Balmer absorption ($W_{H\delta} > 5 \text{ \AA}$) and Balmer break, characteristic of this population.

For further verification, we also determine $W_{H\delta}$ for additional PSB/red-sequence candidates using the lower-resolution spectra available from UDSz (the spectroscopic component of the UDS; see Bradshaw et al. 2013; McLure et al. 2013). Wild et al. (2014) used UDSz for the initial verification of the SC method, but only used spectra from a limited redshift range ($0.9 < z < 1.2$; 5 PSBs). Here, however, we re-analyse the UDSz data using spectra from a wider redshift range ($0.5 < z < 1.4$). Using only good-quality spectra ($S/N > 7$), we find that the majority (9/11; ~ 80 per cent) of PSB candidates exhibit strong Balmer absorption ($W_{H\delta} > 5 \text{ \AA}$), whereas the majority (64/70; ~ 90 per cent) of red-sequence galaxies do not. These UDSz results are in strong agreement with those from our new higher-resolution VIMOS spectroscopy.

In Fig. 3, we show the SC1–SC2 diagram used to identify PSB candidates in the UDS, and highlight the location of our spectroscopically confirmed candidates (based on $W_{H\delta}$ only). Overall, confirmed PSBs span the full range of SC space used for their photometric selection, with the low contamination level in this region indicating the general effectiveness of the demarcations between PSBs, red-sequence galaxies (Red), and star-forming galaxies (SF). Combining results from our new spectroscopy with UDSz, we confirm that 19/24 (~ 80 per cent) of our photometrically-selected PSB candidates exhibit PSB spectral signatures (note: there is minimal overlap between these spectroscopic samples; 1 PSB and 1 Red). We also determine that the overall completeness in photo-

Table 1. Post-starbursts classified from the new higher-resolution VIMOS spectroscopy. Post-starbursts identified from both the SC-selected PSB and red-sequence samples are shown, corresponding to the filled blue circles in Fig. 3. Errors in $W_{H\delta}$ (1σ) are determined from the $W_{H\delta}$ variance between simulated stacks of the 7 OB spectra generated via a bootstrap method.

DR8 ID	RA	Dec	z_{spec}	K_{AB}	$W_{H\delta}(\text{\AA})$
SC-PSB					
68297	34.55707	−5.21842	1.122	20.2	6.3 ± 0.3
68884	34.36123	−5.21409	0.913	22.6	9.5 ± 3.3
75927	34.36846	−5.18122	0.651	22.6	7.2 ± 0.9
76989	34.38889	−5.17662	0.987	21.4	10.1 ± 0.4
96124	34.30828	−5.08844	1.147	20.8	8.2 ± 0.5
96779	34.58438	−5.08598	1.003	20.4	6.5 ± 0.4
97148	34.33352	−5.08409	1.273	20.5	15.2 ± 0.4
102822	34.30597	−5.05690	0.539	20.9	8.9 ± 0.6
105014	34.39562	−5.04624	1.193	21.2	10.5 ± 0.9
118108	34.32720	−4.98463	1.398	20.8	9.6 ± 1.6
118145	34.58369	−4.98389	1.095	21.3	9.3 ± 0.5
SC-Red					
67085	34.42245	−5.22267	0.643	22.3	6.6 ± 0.9
80264	34.37355	−5.16323	1.091	20.0	6.3 ± 0.8
83492	34.54693	−5.14707	1.138	20.3	8.0 ± 0.5
86288	34.58442	−4.13321	0.571	21.4	7.5 ± 0.7
98931	34.52746	−4.07677	1.270	20.1	9.8 ± 0.8
105911	34.35717	−5.04253	1.148	20.1	5.2 ± 0.7
118886	34.34184	−4.98142	1.097	20.1	7.4 ± 0.5
119803	34.35894	−4.97603	1.024	21.8	8.1 ± 1.7

metric PSB selection is ~ 60 per cent, with some spectroscopically confirmed PSBs appearing in the photometric red-sequence population. However, as previously noted, this level of completeness is not unexpected, since the photometric PCA method will naturally be less sensitive to PSB signatures than using spectroscopy.

With respect to these results, an important consideration is that we do not impose a lack of [O II] emission in our PSB criteria. [O II] emission is not considered typical for PSBs; however, we do not use this as a classification criterion to avoid a potential bias against PSBs hosting AGN (Yan et al. 2006). In addition, some [O II] emission may actually be expected in PSBs where star formation was not quenched on a rapid timescale. For our confirmed PSBs, a small number do exhibit significant [O II] emission ($W_{[\text{OII}]} < -10 \text{ \AA}$; 3 galaxies – #68884, #75927, and one candidate from UDSz). However, if we exclude these cases, our confirmation rate for photometrically-selected PSBs only drops to 16/24 (~ 65 per cent). Furthermore, even using a much stricter criterion for [O II] emission ($W_{[\text{OII}]} < -5 \text{ \AA}$; e.g. Tran et al. 2003), we still find that 14/24 (~ 60 per cent) can be confirmed as genuine PSBs. From these results, we conclude that the photometric selection of PSB galaxies is highly effective with, depending on the precise classification criteria used, between 60–80 per cent of the candidates showing spectral signatures characteristic of this population.

Taken together, our results show that the PCA selection of PSBs is highly successful for candidates within the magnitude range of our spectroscopic samples ($K_{\text{AB}} < 23$). However, we note that the PCA selection currently yields PSB candidates down to $K_{\text{AB}} = 24$ (see Fig. 1). At present, we do not have spectra for these fainter candidates to confirm their nature. However, based on their super-colour distributions (i.e. SC1, SC2), there is no indication that these fainter candidates are intrinsically different to those with $K_{\text{AB}} < 23$. Consequently, provided sufficient S/N in the spectra, we anticipate a similar success rate among this fainter population.

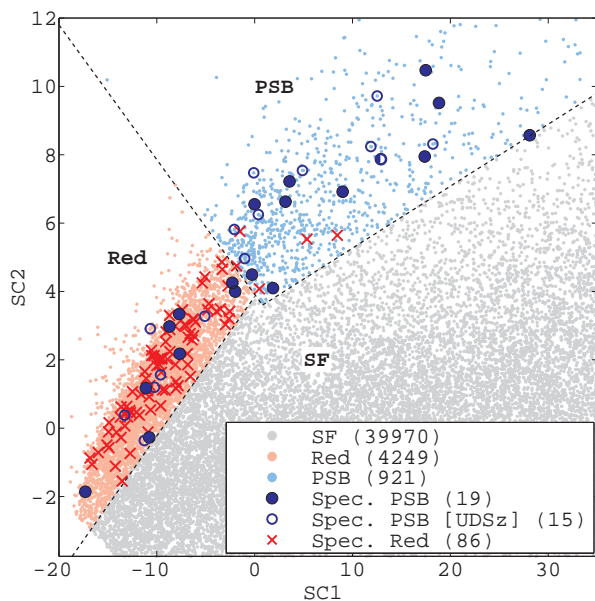


Figure 3. A super-colour (SC) diagram for galaxies in the UDS field ($0.5 < z < 2.0$), showing our spectroscopically confirmed post-starbursts (PSB). The photometrically-selected populations (star-forming, red-sequence and PSB) are indicated by small grey, red and blue points, respectively. We also highlight: i) confirmed PSBs from the latest VIMOS spectroscopy ($W_{H\delta} > 5 \text{ \AA}$; filled blue circles); ii) confirmed PSBs from UDSz (open blue circles); and iii) confirmed red-sequence galaxies ($W_{H\delta} < 5 \text{ \AA}$; red crosses). Sample sizes are shown in the legend.

4 CONCLUSIONS

We present spectroscopic verification of the selection of high-redshift ($z > 0.5$) PSB galaxies from a new photometric technique, based on the PCA analysis of galaxy SEDs. Using deep-optical spectroscopy, we demonstrate the overall effectiveness of this method, with the majority of PSB candidates targeted (~ 80 per cent) exhibiting the strong Balmer absorption ($W_{H\delta} > 5 \text{ \AA}$) and Balmer break, characteristic of this population. Furthermore, using stricter criteria, excluding those with significant [O II] emission ($W_{[OII]} < -5 \text{ \AA}$), we still find a significant fraction of PSB candidates (~ 60 per cent) can be classified as genuine PSBs. However, we caution that using the latter criteria may bias against PSBs hosting AGN, or those with residual star formation. We conclude that the PCA technique and its application to the UDS field are highly-effective in selecting large samples of PSBs at high redshift.

The verification presented of the photometric selection of high-redshift post-starbursts will enable a wide range of science in both the UDS and other deep surveys from large photometric samples. Such studies will be the subject of forthcoming publications, including explorations of their large-scale clustering (Wilkinson et al., in preparation), environments (Socolovsky et al., in preparation), mass-functions (Wild et al., in preparation) and morphology (Almaini et al. submitted; Maltby et al., in preparation).

From our new higher-resolution spectroscopy, we also provide a secure sample of 19 high-redshift PSB spectra for future study. In addition, our re-analysis of the lower-resolution UDSz spectra has yielded an additional 14 PSB spectra, increasing the number of post-starbursts spectroscopically classified in the UDS field from 5 to 33 galaxies. A full analysis of the spectral features for these post-starbursts is beyond the scope of this study, and will be the subject of future publications. However, we do make one initial

observation. Although we do observe some PSBs with significant [O II] emission, we observe no significant signs of AGN activity in the spectra of our post-starburst galaxies (i.e. no high-ionisation emission lines, e.g. [Ne V]). For some quenching models, the presence of an AGN is required to linger past the termination phase to sweep up any remaining gas (e.g. Hopkins 2012). At present we find no evidence for lingering AGN activity in our data, but further work will be necessary to determine the prevalence of obscured and/or low-luminosity AGN in this important transition population.

5 ACKNOWLEDGEMENTS

This work is based on observations from ESO telescopes at the Paranal Observatory (programmes 094.A-0410 and 180.A-0776). RJM acknowledges the support of the European Research Council via the award of a Consolidator Grant (PI McLure). We thank the staff at UKIRT for their efforts in ensuring the success of the UDS project.

REFERENCES

- Baldry I. K., Glazebrook K., Brinkmann J., Ivezić Ž., Lupton R. H., Nichol R. C., Szalay A. S., 2004, *ApJ*, **600**, 681
- Best P. N., Kauffmann G., Heckman T. M., Brinchmann J., Charlot S., Ivezić Ž., White S. D. M., 2005, *MNRAS*, **362**, 25
- Bradshaw E. J., et al., 2013, *MNRAS*, **433**, 194
- Bruzual G., Charlot S., 2003, *MNRAS*, **344**, 1000
- Dekel A., Birnboim Y., 2006, *MNRAS*, **368**, 2
- Diamond-Stanic A. M., Moustakas J., Tremonti C. A., Coil A. L., Hickox R. C., Robaina A. R., Rudnick G. H., Sell P. H., 2012, *ApJ*, **755**, L26
- Dressler A., Gunn J. E., 1983, *ApJ*, **270**, 7
- Freudling W., Romaniello M., Bramich D. M., Ballester P., Forchi V., García-Dabó C. E., Moehler S., Neeser M. J., 2013, *A&A*, **559**, A96
- Furusawa H., et al., 2008, *ApJS*, **176**, 1
- Garilli B., Fumana M., Franzetti P., Paioro L., Scodreggio M., Le Fèvre O., Paltani S., Scaramella R., 2010, *PASP*, **122**, 827
- Goto T., 2007, *MNRAS*, **381**, 187
- Goto T., et al., 2003, *PASJ*, **55**, 771
- Gunn J. E., Gott III J. R., 1972, *ApJ*, **176**, 1
- Hartley W. G., et al., 2013, *MNRAS*, **431**, 3045
- Hopkins P. F., 2012, *MNRAS*, **420**, L8
- Hopkins P. F., Hernquist L., Cox T. J., Di Matteo T., Martini P., Robertson B., Springel V., 2005, *ApJ*, **630**, 705
- Larson R. B., Tinsley B. M., Caldwell C. N., 1980, *ApJ*, **237**, 692
- Lawrence A., et al., 2007, *MNRAS*, **379**, 1599
- Martig M., Bournaud F., Teyssier R., Dekel A., 2009, *ApJ*, **707**, 250
- McLure R. J., et al., 2013, *MNRAS*, **428**, 1088
- Paioro L., Franzetti P., 2012, SGNAPS: Software for Graphical Navigation, Analysis and Plotting of Spectra, Astrophysics Source Code Library (ascl:1210.005)
- Simpson C., et al., 2012, *MNRAS*, **421**, 3060
- Simpson C., Westoby P., Arumugam V., Ivison R., Hartley W., Almaini O., 2013, *MNRAS*, **433**, 2647
- Tran K.-V. H., Franx M., Illingworth G., Kelson D. D., van Dokkum P., 2003, *ApJ*, **599**, 865
- Trujillo I., et al., 2006, *MNRAS*, **373**, L36
- Vergani D., et al., 2010, *A&A*, **509**, A42
- Whitaker K. E., van Dokkum P. G., Brammer G., Franx M., 2012, *ApJ*, **754**, L29
- Wild V., Walcher C. J., Johansson P. H., Tresse L., Charlot S., Pollo A., Le Fèvre O., de Ravel L., 2009, *MNRAS*, **395**, 144
- Wild V., et al., 2014, *MNRAS*, **440**, 1880
- Yan R., Newman J. A., Faber S. M., Konidaris N., Koo D., Davis M., 2006, *ApJ*, **648**, 281

This paper has been typeset from a $\text{\TeX}/\text{\LaTeX}$ file prepared by the author.